Organic & Biomolecular Chemistry

ROYAL SOCIETY OF CHEMISTRY

PAPER

View Article Online
View Journal

Cite this: DOI: 10.1039/d5ob00406c

A self-assembled fluorescent probe for H_2O_2 detection in NAFLD diagnosis

Mengzhao Zhang,[a] Junlei Hao,[b] Chengcheng Wu,[a] Suntao Shi,[a] Zhengyu Ma,[a] Xiaowen Ren,[a] Fei Han,[a] Jiang Wu,[b] Haijuan Zhang*[a] and Baoxin Zhang *[a]

Received 6th March 2025,
Accepted 12th August 2025

DOI: 10.1039/d5ob00406c

rsc.li/obc

Nonalcoholic fatty liver disease (NAFLD) is an epidemic metabolic disorder of the liver involving a constellation of pathological processes. There is accumulating evidence that oxidative stress is an influential mechanism leading to NAFLD. Hydrogen peroxide (H_2O_2) is a major ROS molecule involved in many biological processes in the human body and one of the primary triggers of oxidative stress. Consequently, the monitoring of alterations in H_2O_2 levels within organisms is imperative for research pertaining to NAFLD. Herein, we have tailored and synthesized **CM-CN**, a novel fluorescent probe for the detection of H_2O_2 without autofluorescence, which is capable of interacting with H_2O_2 and then spontaneously generating iminocoumarins with high red emissive fluorescence based on a cascade reaction. Furthermore, the probe demonstrated excellent performance, including a low detection limit (LOD = 44.362 nM) and a large Stokes shift ($\Delta\lambda > 100$ nm). In addition, it exhibited the capacity to monitor alterations in H_2O_2 levels in zebrafish and mouse models of NAFLD. These results illustrate the great potential of this probe as a transformative tool that could advance fundamental research in reactive oxygen species biology, especially in hepatic steatosis and oxidative stress-related diseases.

1. Introduction

Non-alcoholic fatty liver disease (NAFLD) is a common liver metabolic disorder characterized by the accumulation of fat in the liver. If left untreated, it may progress to steatohepatitis, cirrhosis, and even hepatocellular carcinoma.[1–4] The pathological processes of this disease are complex, with oxidative stress playing a crucial role in the onset and progression of NAFLD.[5–8] Hydrogen peroxide (H_2O_2), one of the ROS molecules, plays a pivotal role in numerous biological processes within the body and is recognised as a significant contributor for the onset of oxidative stress.[9–12] Accumulating proofs reveal that one of the most important mechanisms contributing to NAFLD is oxidative stress.[13–17] Hence, there is a pressing necessity for a methodology capable of precise detection of hydrogen peroxide in the liver, thereby facilitating the comprehension of liver-related pathologies and the development of therapeutic interventions.

Fluorescent probes have proven to be exceptionally advantageous in the identification of biological small molecules, protein labeling and disease diagnostics, establishing themselves as some of the most convenient and sought-after tools for exploring complex biological processes.[18–22] At present, many fluorescent probes have been widely used for detecting H_2O_2 in living cells. It is evident that these probes have demonstrated remarkable advancements in multiple fronts. Examples of such properties include extremely rapid response times and superior biomonitoring capabilities resulting from NIR emission, *etc.*[23–26] However, there are certain challenges persisting for these probes, particularly the interference from the background fluorescence of the probe, which has the potential to affect the accuracy of bioimaging studies. Consequently, there is an urgent requirement for a novel probe capable of effectively eliminating background fluorescence interference and enhancing detection accuracy.[27–30]

With the above considerations, we have conceived and synthesized a probe **CM-CN** that can be activated by H_2O_2 based on a cascade intramolecular cyclization reaction, which is different from the common fluorescent probes that use various groups to quench the luminescence effect of the fluorophore (Table S1), instead of constructing a series of specific structures to enable the probe, which is devoid of fluorophores, to generate fluorophores to produce fluorescence by a self-assembled tandem cyclisation reaction after reacting with the detector[31–35] (Fig. 1). Therefore, in comparison with alternative probes, **CM-CN** is not subject to interference from probe autofluorescence and exhibits reduced interference in bioimaging, rendering it more suitable for bioimaging applications. The probe interacts with H_2O_2 and generates a cou-

[a]State Key Laboratory of Applied Organic Chemistry and College of Chemistry and Chemical Engineering, Lanzhou University, Lanzhou 730000, China
[b]Key Laboratory for Tibet Plateau Phytochemistry of Qinghai Province, College of Pharmacy, Qinghai Minzu University, Xining 810007, Qinghai, P. R. China

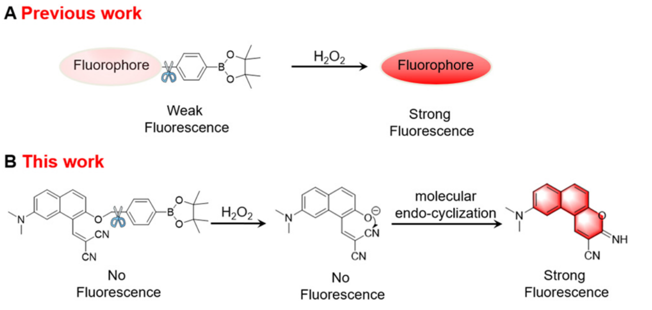

Fig. 1 (A) Traditional strategy of probe design. (B) Our novel strategy of probe design by cascade self-assembly.

marin derivative by intramolecular cyclization. The conjugation between the electron-donating amino group and the electron-withdrawing cyano group in this coumarin derivative endows it with an intramolecular charge transfer (ICT) effect, which results in a large Stokes shift for this fluorophore. A sequence of tests was performed to validate the performance of the probe. The results showed that **CM-CN** exhibits excellent detection and selectivity for H_2O_2, with no background fluorescence and low probe toxicity, which indicates that it is suitable for bioimaging. It is worth noting that the probe could be used to monitor changes in H_2O_2 concentration *in vivo* through fluorescence imaging and noninvasively characterize fatty liver in mice, thereby differentiating between healthy and fatty liver states. Hence, the probe enhances early detection and monitoring of H_2O_2-related diseases such as fatty liver by being responsive to changes in H_2O_2.

2. Experimental section

2.1. Materials and instruments

All chemical precursors employed in organic synthesis met analytical grade specifications, procured through the Titan Discovery platform without requiring additional purification. Reagents were commercially sourced unless otherwise specified, with all solvents subjected to standard purification protocols prior to experimental use. Cell culture components, including Dulbecco's modified Eagle's medium (DMEM) and fetal bovine serum were sourced from Wuhan Pricella Biotechnology Ltd., while chromatographic-grade silica gel was supplied by Yantai Xinnuo New Material Technology Ltd. Biological materials comprised HepG2 hepatocytes (acquired from Lanzhou University School of Medicine), zebrafish strains (Experimental Zebrafish Germplasm Resource Centre), and specific pathogen-free (SPF) male Kunming mice (Laboratory Animal Centre of Lanzhou University). Structural characterization was performed using Bruker nuclear magnetic resonance spectrometers ($^1H/^{13}C$ NMR) complemented by Thermo Scientific high-resolution mass spectrometry. Optical properties were analyzed *via* Thermo Scientific 220 UV-Vis spectrophotometry and Agilent fluorescence spectrophotometry. Subcellular fluorescence imaging utilized a Zeiss LSM 880 NLO confocal microscope, while *in vivo* biodistribution studies employed a Bruker Xtreme II imaging system with multispectral capabilities. The experimental protocols that involved the use of animals were conducted in accordance with the Guidelines for the Care and Use of Laboratory Animals established by the National Institutes of Health and were approved by the Ethics Committee of Lanzhou University.

2.2. Synthesis of CM-CN

The synthetic routes of **CM-CN** are illustrated in Scheme 1. The specific synthetic steps, as well as their compound characterisation, are elucidated in the SI.

2.3. Spectrometric analysis

Stock solutions of **CM-CN** were prepared at 1 mM concentration through dissolution in dimethyl sulfoxide (DMSO), followed by storage under dark conditions at −20 °C. Working solutions were prepared by diluting the stock solution with phosphate-buffered saline (PBS, pH 7.4) to achieve a final concentration of 100 μM, which were subsequently subjected to spectroscopic characterization, including fluorescence emission and UV-visible absorption measurements. To assess the probe's selectivity profile, potential interferents ($CuNO_3$; $CuSO_4$; $FeCl_2$; $FeCl_3$; KNO_3; Na_2CO_3; NaCl; NaHS; $NaHSO_3$; Glu; Thr; Als; Lys; Leu; Pro; Arg; Ser; Gln; His; Met; Asn; Cys; Tyr; O^{2-}; Val; Asp; Hcy; GSH; lle; Gly; Phe; Trp; OCl^-; TBHP; AAPH; ˙OtBu; ˙OH; NO; $^1O_2$; $ONOO^-$) were individually prepared at 1 mM concentration in ultrapure water and introduced into the probe solution for interference testing.

2.4. Cytotoxicity assay and cell imaging

The experimental procedures utilized HepG2 cell models maintained in DMEM-based culture medium (enriched with 10% thermally inactivated fetal bovine serum from Pricella) containing 1% antibiotics (Sangon; 100 U mL^{-1} penicillin and 100 μg mL^{-1} streptomycin). All cell cultures were maintained under standardized conditions: a humidified atmosphere containing 5% CO_2 at 37 °C.

Cell viability assessment was performed through CCK-8 cytotoxicity analysis (Cell Counting Kit-8, Adamas-life) to evaluate the biological effects of **CM-CN**. Cell suspensions (1×10^4 cells per well) were plated in 96-well culture plates containing

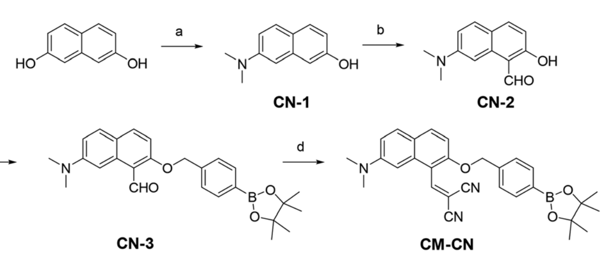

Scheme 1 The synthetic route of **CM-CN**. Reagents and conditions: (a) dimethylamine, $Na_2S_2O_5$, H_2O, 140 °C; (b) $POCl_3$, DMF, 50 °C; (c) 4-(bromomethyl)benzeneboronic acid pinacol ester, K_2CO_3, 85 °C; (d) malononitrile, piperidine, CH_3COOH, EtOH, 85 °C.

100 μL of complete growth medium and maintained under standard culture conditions (37 °C, 5% CO_2). Following 12 h of incubation to ensure cell adhesion, the culture supernatant was aspirated and replaced with fresh DMEM basal medium. **CM-CN** solutions were administered at varying concentrations (12.5, 25, 50, 100, and 200 μM) for 12 h exposure. Post-treatment, cell metabolic activity was quantified by replacing the medium with 100 μL of CCK-8 working solution (10% v/v) and incubating for 60 min. Optical density measurements were conducted at 460 nm wavelength using a Thermo Scientific microplate spectrophotometer.

The fluorescence-based monitoring of H_2O_2 level alterations in HepG2 cells was conducted using a standardized cell treatment protocol. Cell models were subjected to pretreatment with 2 mM H_2O_2 in complete growth medium for 30 min, followed by three cycles of PBS washing (10 mM, pH 7.4) prior to 60 min of incubation with 50 μM **CM-CN**. The parallel control group was directly exposed to **CM-CN** without undergoing oxidative stimulation. Cellular imaging was performed using a laser-scanning confocal microscope, simultaneously capturing bright-field images and red fluorescence emission images for the analysis of hydrogen peroxide dynamics.

2.5. Zebrafish imaging experiment

For *in vivo* fluorescence analysis, larval zebrafish at 3 days post-fertilization were anesthetized and precisely positioned in specialized confocal imaging chambers. The experimental design incorporated three distinct treatment protocols: the first group received direct exposure to 50 μM **CM-CN** for 60 min; the second group underwent sequential pretreatment with 2 mM H_2O_2 for 30 min followed by 60 min of incubation with **CM-CN**; and the third group was initially treated with 20 μM dexamethasone (DXM) for 30 min before 60 min of **CM-CN** incubation. Following probe incubation, all specimens were subjected to gentle PBS washing cycles and subsequently immobilized in imaging chambers containing minimal essential culture medium. Fluorescence acquisition was conducted using a confocal laser scanning microscope equipped with a 10× magnification objective.

2.6. Living mouse imaging experiment

A murine model of NAFLD was established through combined administration of a high-fat diet (HFD) and daily intraperitoneal injections of DXM (100 mg kg^{-1}). Control animals received equivalent volumes of saline injections and standard chow. Following the 7-day induction period, all subjects were administered **CM-CN** (100 mg kg^{-1}) for *in vivo* hydrogen peroxide monitoring. Longitudinal fluorescence imaging was conducted using a small animal *in vivo* imaging system (IVIS) to quantify temporal changes in fluorescence intensity distribution.

3. Results and discussion

3.1 Probe design

An effective fluorescent probe must exhibit high sensitivity and stability, demonstrating significant variations in fluorescence intensity across different concentrations of H_2O_2. Additionally, minimizing the intrinsic fluorescence interference from the probe itself is an essential consideration. Consequently, the selection of a molecular structure with superior fluorescence characteristics is of paramount importance. In this study, we reported the rational design and successful synthesis of a novel cascade reaction-based fluorescent probe, designated as **CM-CN**. The molecular architecture integrates α,β-unsaturated malononitrile moieties covalently conjugated to a naphthalene core through C–C bond formation, while *p*-phenylborate groups are strategically incorporated as H_2O_2-responsive elements *via* ether linkages at the molecular periphery.

The operational mechanism of **CM-CN** involves three sequential transformations: firstly, upon H_2O_2 exposure, the borate ester undergoes specific cleavage to generate a phenolic intermediate, which subsequently undergoes quinone methide elimination. This is followed by a spontaneous intramolecular cyclization process, in which the liberated phenolic group initiates a nucleophilic attack on the adjacent cyano functionality, ultimately yielding a coumarin fluorophore.

The probe's structural sophistication is further enhanced by a dimethylamino substituent positioned on the naphthalene system. This precisely engineered configuration enables effective conjugation between the electron-donating amino group and the electron-withdrawing carbonyl group in the coumarin product, establishing a robust ICT effect that manifests an exceptionally large Stokes shift ($\Delta\lambda$ > 100 nm).[36,37]

With the above design philosophy, the probe that we have designed not only has a significant advantage in terms of H_2O_2 response but also exhibits no interference from the background fluorescence of the probe itself. These combined attributes make **CM-CN** particularly suitable for high-resolution fluorescence imaging applications. The probe's demonstrated capability for real-time H_2O_2 tracking in hepatic systems shows particular promise for investigating pathological mechanisms in fatty liver disease and associated metabolic disorders, potentially enabling new approaches for early clinical intervention.

3.2. Spectroscopic properties of CM-CN

In order to validate the potential of **CM-CN** for H_2O_2 fluorescence imaging, an investigation was conducted into the photophysical characteristics of the probe before and after H_2O_2 exposure under various conditions. Initially, the temporal response profile of the probe to a fixed H_2O_2 concentration (1 mM) was assessed, with the corresponding experimental results presented in Fig. 2A and B. Upon H_2O_2 treatment, the probe exhibited a significant fluorescence enhancement, demonstrating a time-dependent increase that reached maximum intensity after 60 min of incubation, followed by signal stabilization. The fluorescence amplification factor was found to be approximately 24-fold, indicating both excellent H_2O_2 responsiveness and time dependence of the probe. For evaluating the temporal stability of **CM-CN**, an *in vitro* stability experiment was performed (Fig. S1), in which **CM-CN** (100 μM) was incubated with H_2O_2 (1 mM) for 3 h, 6 h, and 9 h, and the

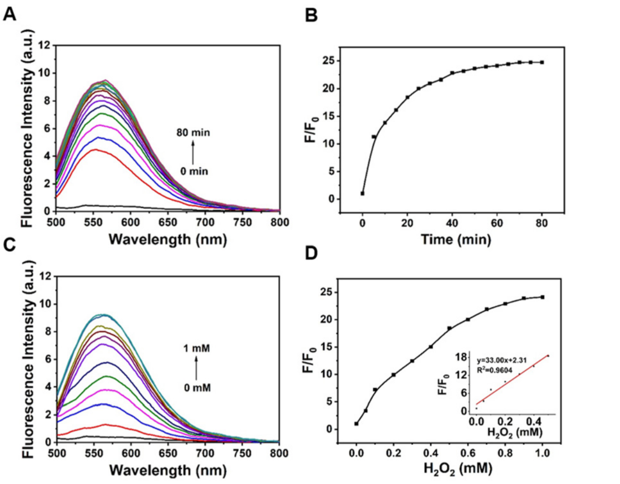

Fig. 2 (A) Fluorescence spectra of **CM-CN** (100 μM) incubated for different times (0–80 min) with H_2O_2 (1 mM). (B) Linear correlation of **CM-CN** (100 μM) incubated for different times (0–80 min) with H_2O_2 (1 mM). (C) Fluorescence spectra of **CM-CN** (100 μM) incubated with different concentrations of H_2O_2. (D) Linear correlation of **CM-CN** (100 μM) in response to H_2O_2 (0–1 mM).

fluorescent signal was monitored for 9 h without any attenuation, confirming that **CM-CN** has significant temporal stability.

In an effort to ascertain the concentration-dependent response of **CM-CN** to H_2O_2, a meticulous evaluation of its fluorescence behavior under varying H_2O_2 concentrations was conducted under a series of standardized experimental conditions. As demonstrated in Fig. 2C and D, the fluorescence emission intensity at 565 nm exhibited a progressive enhancement that correlated with increasing H_2O_2 concentrations, achieving maximal amplification approximately 22.5-fold at 1 mM H_2O_2. Furthermore, quantitative analysis revealed a strong linear correlation between fluorescence intensity and H_2O_2 concentrations within the 0–1 mM range. The detection limit was calculated as 44.362 nM through standard deviation analysis (eqn (S1)). These findings collectively demonstrated that **CM-CN** possesses superior sensitivity and exhibits a pronounced concentration-dependent detection capability for H_2O_2.

Furthermore, to ascertain the validity of the mechanism proposed in Fig. 1, NMR and HRMS titration experiments were carried out for the reaction of **CM-CN** with H_2O_2. The outcomes of these experiments are encouraging, and the generation of the reaction intermediate and the end-product fluorophore, **CN-4**, was observed in the reaction solution of **CM-CN** with H_2O_2 in both experiments (Fig. S2 and S3). This finding validates the proposed mechanism for the response of **CM-CN** to H_2O_2 and further substantiates the viability and feasibility of the novel strategy that was devised.

3.3. pH stability and interference resistance of CM-CN

Following the attainment of compelling fluorescence outcomes for **CM-CN**, a subsequent evaluation of its performance was conducted. For the assessment of the pH-dependent stability of **CM-CN**, we performed a comprehensive validation of its fluorescence response characteristics in different pH environments. As depicted in Fig. 3A, the probe demonstrated optimal performance within the physiological pH range (6.5–8.5), with peak fluorescence intensity observed at pH 7.4. Acidic conditions were found to significantly compromise the sensing capability, a phenomenon potentially attributable to the deprotonated state of the activated fluorophore under physiological conditions that facilitated favorable cyclization kinetics.[38,39] These findings strongly supported the exceptional suitability of **CM-CN** for physiological H_2O_2 detection and its promising application potential in *in vivo* imaging systems.

The experimental findings collectively demonstrated that **CM-CN** exhibited exceptional sensitivity for H_2O_2 detection while maintaining robust fluorescence responsiveness under physiological pH conditions. Nevertheless, the intricate interplay of biological components *in vivo* necessitated rigorous evaluation of molecular selectivity.[40–42] Systematic interference measurements were performed by co-incubation with various amino acids and ROS derivatives, verifying the immunity of **CM-CN** toward H_2O_2. As evidenced in Fig. 3B, **CM-CN** displayed selective activation specifically toward H_2O_2 among the analytes tested, with minimal cross-reactivity observed toward other bioactive molecules. Notably, the response magnitude of the probe to H_2O_2 significantly exceeded that of other ROS derivatives, exhibiting >2-fold signal superiority. This distinct response profile confirmed the remarkable molecular specificity of the probe, as its ability to detect H_2O_2 remained unaffected by potential biological interferents. Such operational stability and target specificity constituted critical prerequisites for accurate quantification of H_2O_2 in complex biological matrices, ensuring that observed signal variations predominantly reflected genuine H_2O_2 fluctuations rather than environmental artifacts. These combined attributes established **CM-CN** as a reliable molecular tool for investigating H_2O_2-associated pathological mechanisms.

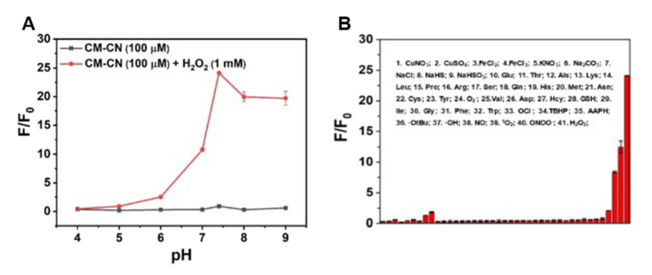

Fig. 3 (A) Fluorescence intensity of **CM-CN** (100 μM) in PBS after adding 0 mM and 1 mM H_2O_2 with different pH values. (B) Fluorescence response of **CM-CN** (100 μM) upon mixing with different species in PBS buffer. 1, $CuNO_3$; 2, $CuSO_4$; 3, $FeCl_2$; 4, $FeCl_3$; 5, KNO_3; 6, Na_2CO_3; 7, NaCl; 8, NaHS; 9, $NaHSO_3$; 10, Glu; 11, Thr; 12, Als; 13, Lys; 14, Leu; 15, Pro; 16, Arg; 17, Ser; 18, Gln; 19, His; 20, Met; 21, Asn; 22, Cys; 23, Tyr; 24, O^{2-}; 25, Val; 26, Asp; 27, Hcy; 28, GSH; 29, Ile; 30, Gly; 31, Phe; 32, Trp; 33, OCl^-; 34, TBHP; 35, AAPH; 36, $^{\bullet}OtBu$; 37, $^{\bullet}OH$; 38, NO; 39, $^1O_2$; 40, $ONOO^-$; 41, H_2O_2. The concentrations of small molecules and proteins were 10 eq. and 1 mM, respectively.

3.4. Intracellular imaging and cytotoxicity activity testing

Prior to biological imaging applications, we conducted rigorous cytocompatibility tests of **CM-CN** using HepG2 cells. Dose–response analysis revealed sustained cell viability exceeding 80% following 12 h exposure to **CM-CN** concentrations of 12.5, 25, 50, 100, and 200 μM (Fig. S4), indicating that **CM-CN** was biocompatible and suitable for use in bioimaging applications. With the aim of accurately assessing the ability of **CM-CN** to monitor the dynamic fluctuations of H_2O_2 in living systems, HepG2 cells were subjected to a standardized treatment consisting of a 30 min pre-treatment with H_2O_2 and 60 min of **CM-CN** incubation, whereas a parallel control group was subjected to **CM-CN** in the absence of oxidative stimuli. Fluorescence imaging analysis (Fig. 4) revealed strong fluorescence in the H_2O_2-treated cells, whereas the other group exhibited only weak basal fluorescence. It was noteworthy that the fluorescence of the H_2O_2-incubated cells was enhanced by a factor of 2.9 when compared to the control group, and these data were also verified by quantitative detection of fluorescence. The residual fluorescence in control specimens likely originated from constitutively expressed reactive oxygen species. This orthogonal validation confirmed the capacity of **CM-CN** for selective exogenous H_2O_2 detection in living cellular environments while maintaining signal fidelity against endogenous interference. The preserved dose–response correlation between *in vitro* and cellular systems established its diagnostic potential for real-time H_2O_2 monitoring, with demonstrated translatability for *in vivo* imaging applications.

3.5. *In vivo* fluorescence imaging in zebrafish

Following the successful demonstration of the capacity of **CM-CN** for intracellular H_2O_2 detection, the investigation was expanded to evaluate its imaging performance in a zebrafish model through validation of both endogenous and exogenous H_2O_2 detection. The experimental design comprised three distinct groups: the negative control group underwent 60 min of incubation with 50 μM **CM-CN** alone; the exogenous H_2O_2 experimental group underwent sequential treatment with 2 mM H_2O_2 (30 min) followed by **CM-CN** incubation; and the endogenous H_2O_2 group was established through DXM-induced fatty liver model development prior to **CM-CN** treatment. Fluorescence imaging analysis (Fig. 5) revealed distinct response patterns: basal fluorescence in the negative control, attributable to constitutive ROS production, and significantly enhanced signals in both experimental groups, with 5.8-fold and 4.8-fold increases for exogenous and endogenous H_2O_2 detection, respectively. The observed 17.2% signal reduction in endogenous *versus* exogenous detection reflected differential H_2O_2 generation mechanisms between pharmacological induction and direct supplementation. These findings collectively demonstrated the capacity of **CM-CN** for precise quantification of both pathologically generated and externally introduced H_2O_2 pools in complex organisms, establishing its diagnostic reliability as a highly sensitive and selective fluorescent probe for *in vivo* applications.

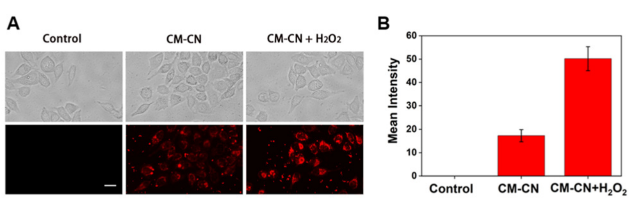

Fig. 4 Fluorescence confocal imaging of HepG2 cells: (A) HepG2 cells were treated with 50 μM **CM-CN** for 60 min; HepG2 cells were treated with 2 mM H_2O_2 for 30 min, and then treated with 50 μM **CM-CN** for another 60 min. (B) Relative fluorescence intensities of the images shown in (A). Data are expressed as mean SEM (bars) (n = 6).

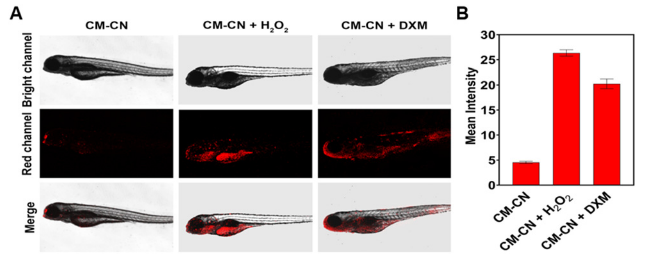

Fig. 5 Confocal laser fluorescence imaging of zebrafish: (A) zebrafish were co-incubated with 100 μM **CM-CN** for 60 min; zebrafish were co-incubated with 1 mM H_2O_2 for 30 min followed by co-incubation with 100 μM **CM-CN** for 30 min; zebrafish were pre-treated with 20 μM DXM for 30 min followed by 100 μM **CM-CN** for another 30 min. (B) The relative fluorescence intensity of the picture from (A). Data are presented as mean SEM (bars) (n = 6).

3.6. *In vivo* fluorescence imaging in mice with fatty liver

It was evident from the extant experimental results that **CM-CN** exhibited exceptional suitability for H_2O_2 monitoring in both cellular and zebrafish models. Building upon these findings, we further validated the capacity of **CM-CN** for real-time H_2O_2 detection in living mice, particularly focusing on its application in NAFLD models. Given the well-established correlation between elevated H_2O_2 levels and hepatic steatosis,[43–46] we established a NAFLD mouse model through high-fat diet (HFD) feeding combined with daily intraperitoneal DXM injections (100 mg kg^{-1}), while control animals received standard chow and saline injections. Following a 7-day induction period, all animals received intraperitoneal **CM-CN** injections (100 mg kg^{-1}) for *in vivo* H_2O_2 monitoring. Fluorescence imaging analysis (Fig. 6) revealed that the fluorescence in the abdomen of NAFLD mice was significantly enhanced compared to the control group, with the strongest signal reaching more than five times that of the control group at the corresponding time point. Furthermore, the signal in the liver region underwent a gradual enhancement over time, with the signal persisting for a duration of 3 h without any discernible dissipation. This observation substantiates the remarkable temporal stability exhibited by **CM-CN**. These findings not only validated the capability of **CM-CN** for real-time H_2O_2 monitoring in complex mammalian systems but also established its potential as a diagnostic tool for evaluating therapeutic efficacy in liver-related pathologies, thereby contri-

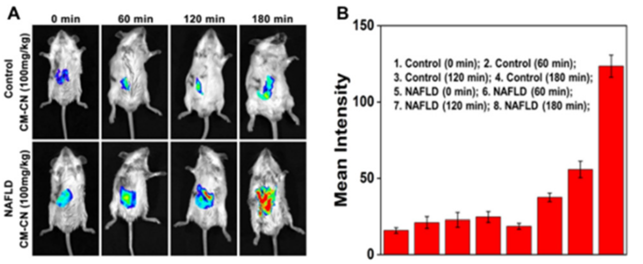

Fig. 6 *In vivo* fluorescence images of mice: (A) normal mice and experimental group mice injected intraperitoneally with **CM-CN** (100 mg kg^{-1}) at 0, 60, 120 and 180 min (λ_{ex} = 460 nm, λ_{em} = 565 nm). (B) The relative fluorescence intensity of the picture from (A). Data are presented as mean SEM (bars) (n = 6).

buting to the development of novel diagnostic and therapeutic strategies for oxidative stress-associated diseases.

4. Conclusions

In conclusion, a fluorescent probe reactive to H_2O_2, designated **CM-CN**, was designed and synthesized, which reacts with H_2O_2, subsequently generating fluorescence *in situ* by means of a self-assembled tandem cyclisation reaction, thus effectively reducing interference from the autofluorescence of the probe. The novel molecular structure under consideration has been demonstrated to offer excellent sensitivity, selectivity and anti-interference properties for the detection of H_2O_2. In addition, **CM-CN** has been observed to exhibit low toxicity and high biocompatibility. Based on these properties, a variety of biological models have been imaged, with the results demonstrating the excellent photostability of the probe and its ability to detect H_2O_2 in bioimaging. These combined attributes position **CM-CN** as a transformative tool for advancing fundamental research in reactive oxygen species biology and clinical translation of redox-targeted therapeutic strategies, particularly in hepatic steatosis and oxidative stress-related disorders.

Author contributions

Mengzhao Zhang: data curation, formal analysis, software, and writing – original draft. Junlei Hao: formal analysis, methodology, and writing – review & editing. ChengCheng Wu: formal analysis and compound synthesis. Suntao Shi: investigation and project administration. Zhengyu Ma: data curation, formal analysis, compound synthesis. Xiaowen Ren: software, writing-review & editing. Fei Han: compound synthesis, investigation, software. Jiang Wu: investigation, funding acquisition. Haijuan Zhang: software, funding acquisition. Baoxin Zhang: funding acquisition, supervision, and writing – review & editing.

Conflicts of interest

The authors declare no conflict of interest.

Data availability

The data supporting this article have been included in the SI. See DOI: https://doi.org/10.1039/d5ob00406c.

Acknowledgements

Financial support from the Natural Science Foundation of Gansu Province (24JRRA384, 25JRRA1125 and 25JRRA667), the National Natural Science Foundation of China (21708017 and 22206067), and the Science and Technology Major Program of Gansu Province of China (22ZD6FA006, 23ZDFA015, and 24ZD13FA017) is acknowledged.

References

1 C. A. Bradley, *Nat. Rev. Gastroenterol. Hepatol.*, 2017, **14**, 139.
2 X. Ren, Z. N. Sayed, S. Shi, J. Hao, J. Gao, J. Wu, H. Zhang, Z. Liu and B. Zhang, *Talanta*, 2025, **286**, 127470.
3 Y. Hu, H. Li, H. Zhang, X. Chen, J. Chen, Z. Xu, H. You, R. Dong, Y. Peng, J. Li, X. Li, D. Wu, L. Zhang, D. Cao, H. Jin, D. Qiu, A. Yang, J. Lou, X. Zhu, J. Niu and Y. Ding, *Nat. Commun.*, 2023, **14**, 6409.
4 N. R. Powell, T. Liang, J. Ipe, S. Cao, T. C. Skaar, Z. Desta, H.-R. Qian, P. J. Ebert, Y. Chen, M. K. Thomas and N. Chalasani, *Nat. Commun.*, 2023, **14**, 1474.
5 S. Han, Y. Zeng, Y. Li, H. Li, L. Yang, X. Ren, M. Lan, B. Wang and X. Song, *Anal. Chem.*, 2023, **95**, 18619–18628.
6 J. Hao, X. Li, S. Shi, H. Zhang, H. Zhu, J. Wu, M. Gao and B. Zhang, *Bioorg. Chem.*, 2025, **155**, 108162.
7 K. Ray, *Nat. Rev. Gastroenterol. Hepatol.*, 2018, **15**, 130–131.
8 B. Hu, Q. Liu, Y. Jiang, Y. Huang, H. Ji, J. Zhang, X. Wang, X.-C. Shen and H. Chen, *Angew. Chem., Int. Ed.*, 2025, **64**, e202418378.
9 M. Abo, Y. Urano, K. Hanaoka, T. Terai, T. Komatsu and T. Nagano, *J. Am. Chem. Soc.*, 2011, **133**, 10629–10637.
10 C. C. Winterbourn, *Nat. Chem. Biol.*, 2008, **4**, 278–286.
11 S. Ye, J. J. Hu and D. Yang, *Angew. Chem., Int. Ed.*, 2018, **57**, 10173–10177.
12 W. Zhang, T. Liu, F. Huo, P. Ning, X. Meng and C. Yin, *Anal. Chem.*, 2017, **89**, 8079–8083.
13 T. Akaike, T. Ida, F. Y. Wei, M. Nishida, Y. Kumagai, M. M. Alam, H. Ihara, T. Sawa, T. Matsunaga, S. Kasamatsu, A. Nishimura, M. Morita, K. Tomizawa, A. Nishimura, S. Watanabe, K. Inaba, H. Shima, N. Tanuma, M. Jung, S. Fujii, Y. Watanabe, M. Ohmuraya, P. Nagy, M. Feelisch, J. M. Fukuto and H. Motohashi, *Nat. Commun.*, 2017, **8**, 1177.
14 I. Leong, *Nat. Rev. Endocrinol.*, 2018, **14**, 190.
15 Q. Zan, K. Zhao, R. Li, Y. Yang, X. Yang, W. Li, G. Zhang, C. Dong, S. Shuang and L. Fan, *Anal. Chem.*, 2024, **96**, 10488–10495.
16 N. Wang, X. Lu, J. Wang, H. Wang, B. Zhang, W. Zhao and J. Zhang, *Anal. Chem.*, 2023, **95**, 5967–5975.

17 S. Peng, B. Zhang, X. Meng, J. Yao and J. Fang, *J. Med. Chem.*, 2015, **58**, 5242–5255.
18 X. Liu, Z. Liu, Y. Li, Y. Wang and W. Zhang, *Org. Biomol. Chem.*, 2025, **23**, 1708–1713.
19 D. Zhu, A. Ren and L. Xue, *Org. Biomol. Chem.*, 2024, **22**, 9113–9120.
20 Z. Yang, Z. Wang, Y. Peng, H. Yang, Q. Wang, X. Jia and X. Liu, *Org. Biomol. Chem.*, 2024, **22**, 8024–8031.
21 S. Das, A. Chaudhuri, H. K. Indurthi, A. K. Agrawal and D. K. Sharma, *Org. Biomol. Chem.*, 2024, **22**, 7332–7336.
22 L. Wang, Y. Huang, J. Wang, Y. Jiang, B.-P. Jiang, H. Chen, H. Liang and X.-C. Shen, *J. Am. Chem. Soc.*, 2025, **147**, 6707–6716.
23 D. Pham, U. Basu, I. Pohorilets, C. M. S. Croix, S. C. Watkins and K. Koide, *Angew. Chem., Int. Ed.*, 2020, **59**, 17435–17441.
24 Q. Zan, K. Zhao, R. Li, Y. Yang, X. Yang, W. Li, G. Zhang, C. Dong, S. Shuang and L. Fan, *Anal. Chem.*, 2024, **96**, 10488–10495.
25 W.-X. Wang, W.-L. Jiang, G.-J. Mao, M. Tan, J. Fei, Y. Li and C.-Y. Li, *Anal. Chem.*, 2021, **93**, 3301–3307.
26 N. Decha, J. Thonglam, J. Meesane, S. Pornsuwan and C. Tansakul, *Org. Biomol. Chem.*, 2024, **22**, 1254–1268.
27 E. W. Miller, A. E. Albers, A. Pralle, E. Y. Isacoff and C. J. Chang, *J. Am. Chem. Soc.*, 2005, **127**, 16652–16659.
28 J. Shin, P. Verwilst, H. Choi, S. Kang, J. Han, N. H. Kim, J. G. Choi, M. S. Oh, J. S. Hwang, D. Kim, I. Mook-Jung and J. S. Kim, *Angew. Chem., Int. Ed.*, 2019, **58**, 5648–5652.
29 D. Kim, S. Singha, T. Wang, E. Seo, J. H. Lee, S.-J. Lee, K. H. Kim and K. H. Ahn, *Chem. Commun.*, 2012, **48**, 10243–10245.
30 J. J. O'Sullivan and M. C. Heffern, *Org. Biomol. Chem.*, 2022, **20**, 6231–6238.
31 L. Meng, Z. Xu, J. Chen, H. Luo and N. Li, *Anal. Chim. Acta*, 2024, **1308**, 342660.
32 C. Luo, Y. Chen, J. Gu, H. Cai, H. Lin, Z. Jin and C. Huang, *Anal. Chem.*, 2024, **96**, 9969–9974.
33 P. Wang, L. Yu, J. Gong, J. Xiong, S. Zi, H. Xie, F. Zhang, Z. Mao, Z. Liu and J. S. Kim, *Angew. Chem., Int. Ed.*, 2022, **61**, e202206894.
34 C. Wu, H. Wei, S. Shi, Z. Wang, Z. Zhang, A. Osama, J. Wu, H. Zhang and B. Zhang, *J. Mater. Chem. B*, 2025, **13**, 2067–2073.
35 K. Ma, L. Zhao, Y. Yue, F. Huo, J. Chao and C. Yin, *Anal. Chem.*, 2020, **92**, 15936–15942.
36 W. Zhang, Q. Jia, Y. Meng, S. Chen, Y. Zhang, K.-P. Wang, L.-H. Gan and Z.-Q. Hu, *Spectrochim. Acta, Part A*, 2020, **228**, 117835.
37 A. Declemy, C. Rulliere and P. Kottis, *Chem. Phys. Lett.*, 1983, **101**, 401–406.
38 H. Wang, J. Guo, T. Xiu, Y. Tan, P. Li, W. Zhang, W. Zhang and B. Tang, *Chem. Sci.*, 2025, **16**, 345–353.
39 D. Maity, A. Raj, P. K. Samanta, D. Karthigeyan, T. K. Kundu, S. K. Pati and T. Govindaraju, *RSC Adv.*, 2014, **4**, 11147–11151.
40 L. Fan, Q. Zan, X. Wang, X. Yu, S. Wang, Y. Zhang, Q. Yang, W. Lu, S. Shuang and C. Dong, *Chem. Eng. J.*, 2022, **449**, 137762.
41 B. C. Dickinson, C. Huynh and C. J. Chang, *J. Am. Chem. Soc.*, 2010, **132**, 5906–5915.
42 X. Bai, Y. Huang, M. Lu and D. Yang, *Angew. Chem., Int. Ed.*, 2017, **56**, 12873–12877.
43 N. Wang, X. Lu, J. Wang, H. Wang, B. Zhang, W. Zhao and J. Zhang, *Anal. Chem.*, 2023, **95**, 5967–5975.
44 B. Zhang, S. Qin, N. Wang, X. Lu, J. Jiao, J. Zhang and W. Zhao, *Talanta*, 2024, **266**, 124971.
45 G. Fan, B. Zhang, J. Wang, N. Wang, S. Qin, W. Zhao and J. Zhang, *Talanta*, 2024, **268**, 125298.
46 J. Liu, X. Liu, Y. Shan, H. Ting, X. Yu, J.-W. Wang and B. Liu, *Biomaterials*, 2024, **306**, 122506.